Submitted to “Geothermics”

3-D resistivity imaging of the supercritical geothermal system in Sengan geothermal region, NE Japan

Yusuke Yamaya[a,*], Yota Suzuki[a], Yasuaki Murata[a], Kyosuke Okamoto[a], Norihiro Watanabe[a], Hiroshi Asanuma[a], Hideaki Hase[b], Yasuo Ogawa[c], Toru Mogi[c], Keiichi Ishizu[c], Toshihiro Uchida[d]

[a]Renewable Energy Research Center, National Institute of Advanced Industrial Science and Technology (AIST), 2-2-9 Machiikedai, Koriyama, Fukushima 963-0298, Japan
[b]Geothermal Energy Research & Development Co., Ltd., Shinkawa Nittei Annex Bldg., 22-4, Shinkawa 1-chome, Chuo-Ku, Tokyo 104-0033, Japan
[c]Volcanic Fluid Research Center, Tokyo Institute of Technology, 2-12-1 Ookayama, Meguro, Tokyo, 152-8551, Japan
[d]Geological Survey of Japan, National Institute of Advanced Industrial Science and Technology (AIST), Hihashi 1-1, Tsukuba, Ibaraki, Japan

[*] Corresponding author: Yusuke Yamaya (y.yamaya@aist.go.jp)

Abstract

A wideband magnetotelluric survey was performed in the Sengan geothermal region of northeastern Japan. A conductor with resistivity of < 30 Ωm was found at a depth of -1.8 km in the Quaternary Kakkonda granite. Microseismic activity was not observed, suggesting a ductile zone with temperatures exceeding 370 °C. Under these conditions, H_2O-NaCl fluids can exist as two-phase or single-phase types. The permeability of the upper reservoir surface is between 5.0E-17 and 5.0E-15 m^2, indicative of an exploitable supercritical geothermal reservoir. Our results indicate that this is originated by heat and water supply system from deep magmatic fluids.

Keywords: Supercritical geothermal system, magnetotellurics, resistivity, permeability, magmatic fluids

1. Introduction

The Sengan geothermal region, located on the volcanic front of the Northeast Japan Arc, is one of the highest geothermal potential areas in Japan. Two geothermal power plants (GPP) are currently in operation in the southeastern part of the region, namely Matsukawa (23.5 MWe), which was the first commercial geothermal power plant in Japan, and Kakkonda (80 MWe). In the Kakkonda area, Quaternary intrusive granite (Kakkonda granite) has been found at a depth of approximately 3 km beneath the currently utilized reservoir. Kakkonda granite is considered the dominant heat source in the Kakkonda area (Doi et al., 1998); the WD-1a well reached the Kakkonda granite at 2,860 m depth, and a temperature of 500–510 °C was confirmed at a depth of 3,720 m (Ikeuchi et al., 1998). The Kakkonda granite is still a cooling intrusive rock whose deeper part is in a state of partial melting (Doi et al., 1998).

The measured temperature at a depth of 3,100 m in the WD-1a well reached 380 °C (Ikeuchi et al., 1998). The pressure must be high at such depths, and the pore water in rocks may be in a supercritical state, possibly forming a supercritical geothermal system (Okamoto et al., 2019). Supercritical geothermal systems are very high-temperature geothermal systems located at depths near or below the brittle-ductile transition zone of the crust, where the reservoir fluid is assumed to be supercritical (Reinsch et al., 2017). These systems have received much attention in recent years as potential unconventional geothermal resources because of their very high enthalpy of the component fluids (Reinsch et al., 2017; Okamoto et al., 2019). However, high-level drilling technology is required to exploit these resources because of the high temperature and pressure conditions at depth (3–5 km) and the expected high corrosivity of the fluids (Reinsch et al., 2017; Yanagisawa et al., 2021). The IDDP2 project in Iceland was the first to reach supercritical geothermal fluids through drilling (Friðleifsson et al., 2017). The state of supercritical geothermal fluids and their surrounding conditions are important issues in research into utilizing such fluids for future power generation. Therefore, it is necessary to drill test wells to collect data on supercritical geothermal fluids and their reservoirs. As an important first step, the promising locations of supercritical geothermal reservoirs must be accurately estimated. It is also necessary to understand the lateral and vertical extent of potential supercritical geothermal systems to evaluate the available resources.

Resistivity surveys can reveal the distribution of fluids in the subsurface. The resistivity of rock is sensitive to the amount of pore water it contains as well as pore water salinity and temperature. The magnetotelluric (MT) method is a resistivity survey technique that exploits natural electromagnetic field variations. The resistivity structure at depths of several hundred meters to several tens of kilometers can be revealed by measuring the electromagnetic (EM) field variation at many stations on the surface over a wide area and analyzing the EM fields in a wide frequency band. In recent years, three-dimensional (3-D) inversion of MT data has become increasingly practical (e.g., Siripunvaraporn et al., 2005; Kelbert et al., 2014; Usui, 2015; Usui et al., 2017), and 3-D resistivity structures can now be accurately estimated. Indeed, electrically conductive structures from the deep subsurface to geothermal and volcanic zones have been found in many locations using 3-D MT surveys (e.g., Ogawa et al., 2014, Bertrand et al., 2015; Yamaya et al., 2017a, Hata et al., 2018; Karlsdóttir, 2020; Lee et al., 2020; Tsen et al., 2020; Ishizu et al., 2021). In most cases, conductive bodies are interpreted as migration paths and stagnation zones of magmatic fluids, including saline fluids and partial melts.

Resistivity structures have also been estimated in the Kakkonda area of the Sengan geothermal region using the MT method (Uchida et al., 2000, 2003; Yamaya et al., 2017b). These studies have commonly estimated the conductive body corresponding to the Kakkonda granite. Yamaya et al. (2017b) used MT data similar to those of Uchida et al. (2003) to estimate the 3-D resistivity structure of the Kakkonda area. These authors found a significant conductor in the interior of the Kakkonda granite at a depth of 3 km or more. Yamaya et al. (2017b) suggested that the resistivity values could be explained by the presence of supercritical geothermal fluids based on their depth and temperature; however, their analyses did not consider topography, and the areal/lateral coverage of the observation stations was limited, which prevented them from discussing the structure at depth in detail. Therefore, MT measurements with observation stations located over a wider area are required along with an analysis that fully considers the topography.

The purpose of this study is to clarify the location and size of the conductive body in the Kakkonda granite, which is expected to be a supercritical geothermal reservoir, and clarify the geothermal fluid supply system in this area by estimating the resistivity structure in deep and wide areas through MT exploration. In addition, a method for estimating permeability—an important parameter for supercritical geothermal reservoir modeling—from resistivity measurements is discussed. Based on the results of these approaches and on geophysical, geological, and geochemical information, we propose that the Kakkonda geothermal area is likely to contain supercritical geothermal reservoirs that can be used for power generation. Thus, this study provides valuable preliminary information to inform future test drilling targeting supercritical reservoirs.

2. Study area

The Sengan geothermal region is located on the volcanic front of the Northeast Japan Arc (Fig. 1), within which the Kakkonda area has the greatest geothermal potential with a current installed capacity of 80 MWe. In this area, liquid-dominant reservoirs have been formed consisting of shallow reservoirs (0–1,500 m) and deep reservoirs (1,500–3,100 m) (Hanano, 1995; Kato et al., 1998). Underneath these geothermal reservoirs sits the Quaternary Kakkonda granite intrusion, which acts as one of the main heat sources. The age of the Kakkonda granite is 0.2 Ma, which means that the magma was cooled during intrusion at a depth of 3 km (Doi et al., 1998). The New Energy and Industrial Technology Development Organization (NEDO) drilled the WD-1a exploration well in 1994–1995, reaching the Kakkonda granite at a depth of 2,860 m and terminating at a depth of 3,729 m (Ikeuchi et al., 1998). The temperature in the well reached 380 °C at a depth of 3,100 m, at which point the temperature profile changed from a hydrothermal convective type to a thermal conduction type (Ikeuchi et al., 1998). At a depth of 3,720 m, a temperature of 500–510 °C was observed (Ikeuchi et al., 1998). Pore water in rock above 380 °C at a depth of 3,100 m can exist in a supercritical state; however, no highly permeable supercritical geothermal reservoirs were identified by the WD-1a drilling. The depth distribution of the Kakkonda granite was subsequently estimated using well data and the microseismic distribution. Doi (2001) estimated the granite to have a symmetrical elliptic shape with its major axis at N30°W, covering an area of approximately 8 × 5 km at 2,200 m below sea level (Fig. 1).

The Matsukawa geothermal area is located approximately 7 km north of the Kakkonda area. The Matsukawa power plant was the first geothermal power plant in Japan, which began operation in 1966 and is currently generating 23.5 MW of electricity. Unlike Kakkonda, this is a steam-dominated geothermal reservoir (Hanano and Matsuo, 1990). Kimbara (1983) considered that the geothermal areas of Kakkonda and Matsukawa are related because of the distribution of alteration zones, and estimated that they share the same heat source, located beneath the Kakkonda geothermal area.

The active Iwate volcano is located in the eastern part of the study area, with a seismic swarm and crustal deformation since 1995. In September 1998, a M6.1

earthquake occurred at the southwestern foot of the volcano followed by a sharp decline in seismic activity. The migration of the seismic source distribution coincided with the pressure source of the geodetic deformation, suggesting that magma was supplied from the deep subsurface. Aizawa et al. (2009) estimated the resistivity cross-section of the Iwate volcano by conducting MT and audio-frequency MT (AMT) surveys. These authors identified a resistive body beneath the summit and interpreted this as a past, solidified magma intrusion that prevented new magma from moving upward, resulting in a westward migration.

3. Methods

3.1. Survey of existing resistivity structures

Uchida et al. (2000; 2003) analyzed MT data measured in the Kakkonda area, assuming 2-D and 3-D structures. As a result, they estimated a relatively conductive body corresponding to the Kakkonda granite. Yamaya et al. (2017b) pointed out that the 3-D analysis by Uchida et al. (2003) was insufficient because they did not use the diagonal component of the impedance, and performed a 3-D inversion analysis using the full impedance components of the existing MT data. As a result, a remarkably sharp conductor was estimated for the Kakkonda granite. The estimated resistivity was as low as 10 Ωm, which is difficult to explain without the presence of conductive pore water or melt. Considering a temperature of 400–500 °C and lithostatic pressure at approximately 2,500 m depth, Yamaya et al. (2017b) suggested that a supercritical reservoir may exist. They did not, however, consider topography, meaning that the depth of the low-resistivity body remains uncertain. In addition, the size of the conductor was not well determined because it extended outside of the observed area (survey area) and at depths where there was no sensitivity. Building on this work, we added new high-quality MT data and performed 3-D analysis considering the topography. We also extended the scope of analysis to examine the relationships between deeper and wider structures, and considered whether similar structures exist in other locations (Fig. 2).

3.2. MT data

To cover the eastern part of the Sengan region including the Kakkonda and Matsukawa areas, existing and newly measured MT data were used. We assumed that the resistivity structure did not change during the observation period. The new MT data were measured in 2017, 2019, and 2020, and the distribution of the MT stations is shown in Fig. 2. In the 2017 and 2020 surveys, we used the Metronix ADU-07e system and MFS-06e or MFS-07e induction coils. In the 2019 survey, we used the Phoenix Geophysics MTU-5A system and MTC-50, MTC-80, and MTC-80H induction coils. Pb-PbCl2 electrodes were used for all the electric field measurements. Two components of the electric field and three components of the magnetic field were measured, although the magnetic field measurements were omitted for some mountainous stations.

The time-series data for 2017 and 2020 were processed using the 'BIRRP' software (Chave and Thomson, 2004). Remote reference processing (Gamble et al., 1979) was performed using magnetic data from a station 140 km south-southwest (Station A in Fig. 1). Time-series processing of the 2019 data was performed using the SSMT 2000 system from Phoenix Geophysics, which was remotely referenced to magnetic data from a station approximately 120 km south-southwest (Station B in Fig. 1). The impedance and magnetic field transfer functions were calculated for each station and each frequency between 300 and 0.0003 Hz.

As the study area is considered to have high geothermal potential, various surveys have been conducted since the 1980s, offering several other existing MT datasets (NEDO, 1990, 1999; Ogawa et al., 1997; Uchida et al., 2000; Aizawa et al., 2009). However, because most investigations and analyses were conducted using old equipment and methods, high-quality data are limited. For our study, we checked the quality of the existing data and decided to use the data from the stations shown in Fig. 2 for the 3-D inversion analysis. Figure 3 shows the apparent resistivity calculated from the sum of squared elements (SSQ) invariants of the impedance (Rung-Arunwan et al., 2017) and the induction vector derived from the magnetic field transfer function for the observation station used for the inversion.

3.3. 3-D inversion

The 3-D inversion was performed using 'WSINV3DMT' software (Siripunvaraporn et al., 2005; Siripunvaraporn and Egbert, 2009). The input data consisted of four impedance components from 110 locations, and two components of the magnetic field transfer function from 56 locations with magnetic field data. The error floor was set to 10%, and 16 frequencies between 30 and 0.001 Hz were used. Because several frequency tables were mixed owing to differences in the measurement equipment and data-processing software, the frequencies were represented by the nearest frequencies. The computational grid was 89 (x) × 92 (y) × 71 (z) with a minimum block size of 250 × 250 × 40 m, increasing in size towards the sides and in the downward direction (Fig. 2). The overall model size was 452.5 × 454.5 × 223.5 km. For the initial and prior models, the resistivity of the land area was set to 100 Ωm. Topography was considered based on the numerical elevation model (10 m mesh) developed by Geospatial Information Authority of Japan, and the air resistivity was fixed at 10^8 Ωm. 'ETOPO1' (NOAA National Geophysical Data Center, 2009) and 'J-EGG500' (http://www.jodc.go.jp/data_set/jodc/jegg_intro.html) were used to obtain bathymetry information, and the seawater resistivity was fixed at 0.3 Ωm.

The inversion analysis was conducted in two steps. First, five iterations were performed from the initial structure. The resistivity model with the smallest root-mean-square (RMS) residual between the calculated and observed values was used as the initial and prior models for the second step of the inversion. The model with the smallest RMS residual in the second step was then used as the final model candidate. This procedure was performed by varying τ (Siripunvaraporn and Egbert, 2000; Siripunvaraporn et al., 2005), which determines the model length in 'WSINV3DMT'. The RMS residuals of the final model candidates were 1.292, 1.309, and 1.422 for $\tau = 2.5$, 5.0, and 10, respectively. Because there are many wells in this area where resistivity logging has been conducted, we used the data from surveys reported by New Energy and Industrial Technology Development (NEDO, 1983, 1991, 1992a, 1992b, 1993, 1998) and unpublished data provided by the Tohoku Sustainable & Renewable Energy Co. Inc., Sendai, Japan. The goodness-of-fit between the long-normal resistivity logs at 79 wells and the resistivity of the final model candidate was 196, 144, and 923 Ωm for $\tau = 2.5$, 5.0, and 10, respectively. Given these results, the $\tau = 5.0$ model was selected as the final resistivity model.

The apparent resistivities of the SSQ invariant and induction vector calculated from the final model are shown in Fig. 3; the calculated and observed values are in good agreement. The fits of the apparent resistivity, phase, and magnetic-field transfer functions are shown in Fig. S1. Similarly, the fit between the calculated and observed values is generally good, although for the observed data with large errors, the calculated values have large degrees of freedom. For these stations, future re-measurement is desirable to improve data quality.

3.4. Resistivity model

The plan views and vertical sections of the final model are shown in Figs. 4 and 5, respectively. The general characteristics of the final model are as follows:

- The surface layer of several hundred meters has a high resistivity up to 1,000 Ωm. In the Kakkonda and Matsukawa geothermal areas, conductive layers of less than 10 Ωm are distributed in the shallow part below the surface layer.
- From a few hundred meters to an elevation of -2 km, the eastern side shows a low resistivity layer of approximately 10 Ωm, reflecting the sedimentary layers to the north and south of the Iwate volcano. On the western side, there are resistive layers of several hundred Ωm or more, which correspond to the mountainous topography.
- A high-resistivity layer of approximately 100 Ωm continues at elevations below -3 km.

A remarkable conductor is inferred in the interior of the Kakkonda granite at elevations below 1.8 km (Figs. 5b, 5e, and 10). The resistivity of this conductor is generally less than 30 Ωm, reaching less than 1 Ωm in the central part. Although the resistivity values vary slightly, the location of the relatively low resistivity values is consistent with the results of the existing 3-D analysis of the MT data (Uchida et al., 2003; Yamaya et al., 2017b). The upper part of this conductor is an important structure because it may be a supercritical geothermal reservoir, as the estimated temperature is 380–500 °C (Doi et al., 1998; Fig. 10).

As the extremely low resistivity value at the center of the conductor might be due to the smoothing constraint in the inversion analysis, we examined the sensitivity to this value in more detail. We replaced the part of the resistivity lower than the test resistivity in the frame of Fig. 6 (elevations of -1.8 to 2.6 km, which likely encompasses the main zone of the reservoir) with the test resistivity. The test resistivity was assumed to be 1 to 30 Ωm, and the MT response was calculated. The RMS residuals of the calculated and observed MT responses with respect to the test resistivity are shown in Fig. 7. The larger the test resistivity, the larger the RMS residuals; when the test resistivity was 10 Ωm, the RMS value was 1.326. Models with RMS smaller than this are within the 95% confidence interval of the F-test for MT resistivity models (Ichihara et al., 2014) and can be considered equivalent models. Therefore, it was ensured that the resistivity of the center of the conductor was at least 10 Ωm. Furthermore, because the RMS residuals remained stable when the lower limit of the resistivity was 3 Ωm or less, 3 Ωm was considered the limit at which the resistivity value can be discriminated.

Although previous studies did not detect a deeper extension of the conductor, we estimated that the conductor extends to -10 km beneath the Eboshidake volcano southwest of Kakkonda. The resistivity of this deep extended conductor was determined to be less than 30 Ω m using the F-test. In contrast, no other conductive anomalies were found in the survey area deeper than 3 km below the surface. However, because the observation points around the Iwate volcano were sparse and the data quality in the low-frequency band was poor, deep anomalies may have been missed. As a simple sensitivity test, we embedded a 4-km 1 Ωm conductive cube at an elevation of -2 km or deeper beneath the volcano. However, we found no significant change in the calculated response, nor was the difference significant based on the F-test. As such, detecting a conductive anomaly at this location remains challenging using existing datasets.

3.5. Permeability

For the development of supercritical geothermal reservoirs, it is necessary to create an accurate reservoir model, for which permeability is an important parameter. Here, we attempted to estimate the permeability of the conductive body in the Kakkonda granite based on resistivity and other existing information.

Permeability is related to porosity because water flows only in the pores of rock. Glover et al. (2006) provided the RGPZ (Revil, Glover, Pezard, Zamora) equation to express the following relationships:

$$k_{RGPZ} = \frac{d^2 \varphi^{3m}}{4am^2} \ , \qquad (1)$$

where d is grain size; φ is porosity; a is a constant related to particle packing, which is usually approximated as 8/3; and m is the cementation factor given by Archie's (1942) equation:

$$F = \frac{\rho_b}{\rho_w} = a\varphi^{-m} \ , \qquad (2)$$

where ρ_b is the resistivity of the rock (bulk resistivity), and ρ_w is the resistivity of the pore water. The ratio of these resistivities, F, is called the formation factor. Substituting Eq. (2) into Eq. (1) gives:

$$k_{RGPZ} = \frac{d^2\varphi^{3m}}{4am^2} = \frac{d^2}{4am^2F^3}. \quad (3)$$

The RGPZ equation (Eq. 3) has been applied to sandstone and mudstone, which constitute petroleum reservoirs but has not been validated in deep-seated rocks. We investigated the applicability of the RGPZ equation using the porosity and permeability measurements of core samples of the Kakkonda granite reported by NEDO (1998) and Fujimoto et al. (2000). Kanisawa et al. (1994) reported that the grain size of the Kakkonda granite was 0.5–1.5 mm. We assumed d = 1 mm and plotted the permeability with respect to porosity based on Eq. (3) for m = 1.5–2.2 (Fig. 8). The relationship based on the RGPZ equation for m = 1.8 fitted the laboratory measurements well, which can be applied to the Kakkonda granite assuming that there is no large-scale fracturing.

Watanabe et al. (2021b) estimated the electrical conductivity of H_2O-NaCl fluids in a supercritical geothermal reservoir based on the assumed temperature, pressure, and salinity in the reservoir, and estimated the bulk resistivity of fluid-saturated rocks. They assumed that m = 1.5 or m =1.8 and φ = 5%. These authors concluded that H_2O-NaCl fluids in supercritical geothermal reservoirs can be vapor-like, two-phase dominant, or single-phase types depending on the reservoir pressure. Additionally, they showed that if the bulk resistivity of the reservoir is less than approximately 30 Ωm, the fluid state is likely to be either the two-phase dominant or single-phase type (Watanabe et al., 2021b). The conductor corresponding to the Kakkonda granite ranges from 3 to 30 Ωm, suggesting a two-phase dominant or single-phase reservoir. In addition, the upper surface of the conductor has a depth of approximately 2.7–3 km. Considering the temperature cross-section of the Kakkonda area reported by Doi et al. (1998) (Fig. 10), the temperature exceeds 380–400 °C at the depth of the upper surface of the conductor (2.7–3 km). These conditions are similar to those considered by Watanabe et al. (2021b); therefore, we estimated permeability using these temperature and pressure conditions.

The two-phase dominated reservoir is assumed to be a moderate pressure condition (> 32 MPa assuming the maximum reservoir temperature is 500 °C; Watanabe et al. 2021b). Because hydrostatic pressure is estimated to be approximately 25 MPa when the temperature reaches 380 °C at a depth of 3 km, the reservoir pressure was assumed to be 35 MPa (+10 MPa). Based on Yanagisawa et al. (2021), the salinity of the pore water was assumed to be 6 wt%. The resistivity of the NaCl water was based on the fitting equation developed by Watanabe et al. (2021a) based on the experiments of Bannard (1975). The resistivity of the 6 wt% NaCl water at 35 MPa and 380–400 °C was 0.036–0.045 Ωm. A resulting permeability corresponding to a bulk resistivity of 3–30 Ωm is calculated when m = 1.8 and d = 1 mm, resulting in the "Hydrostatic" curve shown in Fig. 9. Because the reservoir pressure of the single-phase type is similar to the lithostatic pressure, the reservoir pressure was assumed to be 78 MPa. The corresponding resistivity of 6 wt% NaCl water at 78 MPa and 380–400°C is approximately 0.03 Ωm, and permeability was calculated as the "Lithostatic" curve in Fig. 9. Because the actual pressure in the reservoir may lie between these two curves, the permeability was estimated to be between these two curves.

The permeability corresponding to a bulk resistivity of 3 to 30 Ωm was estimated to be within the range of 5.0E-17 to 1.0E-13 m^2. As resistivity was 10 Ωm or less at the center of the conductor based on the F-test of the resistivity model, we consider a permeability of approximately 5.0E-17 to 5.0E-15 m^2 to be conservative estimate.

4. Results and Discussion

4.1. Conductor in the Kakkonda granite body

A remarkable conductor was estimated in the interior of the Kakkonda granite at an elevation of -1.8 km or deeper (Fig. 10). The resistivity of this conductor is generally less than 30 Ωm and less than 1 Ωm in the central part. Importantly, our resistivity model includes topography, uses wide-area data, and explains the magnetic field transformation function in addition to impedance, meaning that the estimated structure of the conductor is more robust than in previous studies.

Unlike other wells, as the resistivity structure obtained using MT does not match well with the logging data of WD-1a (Supplementary Fig. S2), this well may reflect the resistivity transition zone. The resistivity boundary is probably more complex, or the resistivity contrast is large, but it may be estimated as a smooth boundary owing to the smoothing constraint in the inversion analysis. The resistivity of the logging data is consistently higher than that of the resistivity model, resembling the resistivity structure outside the low-resistivity body. Therefore, WD-1a was probably located outside the conductor and did not, therefore, encounter a supercritical geothermal reservoir. As such, the conductor may have a different physical state from that derived from WD-1a. Indeed, as previously mentioned, a conductor below 30 Ωm at this depth and with a temperature above 380 °C implies a two-phase dominant or single-phase supercritical geothermal reservoir.

Supercritical geothermal reservoirs are thought to be formed by the precipitation of dissolved constituents, such as silica, in fluids released from magma to form caprocks (Fournie, 1999; Tsuchiya et al., 2016). Saishu et al. (2014) estimated the silica solubility profile of WD-1a and showed that the boundary depth between the hydrothermal convection zone and the thermal conduction zone coincides with the depth of the minimum quartz solubility. This indicates that a silica caprock could have formed at this depth. A silica cap would be resistive but may be too thin to be detected at the resolution of the MT method. Therefore, the conductor was analyzed as if connected to the upper conductive zone corresponding to the conventional reservoir. Okamoto et al. (2021) determined highly accurate hypocenters of microearthquakes that occurred in the Kakkonda geothermal area. They further suggested that earthquakes do not occur within the conductive anomaly of Yamaya et al. (2017b) but that it is a ductile zone hotter than 370 °C. Seismic tomography results also suggest that there is no significant flow within the conductor, while fluid may flow laterally within the shallow convective reservoir (Okamoto et al., 2021). In other words, the conductive body within the Kakkonda granite is not hydrologically connected to a shallow reservoir. These results suggest that the conductor in the Kakkonda granite is likely to be a reservoir of supercritical fluids. Based on our analysis, the permeability of the upper part of the conductor at 380–400 °C is estimated to be between 5.0E-17 and 5.0E-15 m^2 or higher, which is viable for steady steam production.

Doi et al. (1998) noted that the deep geothermal gradient of WD-1a is approximately 32 °C/100 m, and the temperature may exceed 800 °C at a depth of 5 km. This suggests that the granite is partially melted at depth. The conductor may, therefore, indicate partial melting and magmatic fluids, including brine, at these depths.

4.2. Geothermal supply system in the Sengan geothermal region

Figure 11 shows a 3-D cut model as a NE-SW cross-section. The conductor corresponding to the Kakkonda granite extends from an elevation of -10 km beneath the Eboshi volcano in the southwest of the Kakkonda area. The cross-section shows that this conductive body diverges at an elevation of -3 to -4 km and extends into the Kakkonda granite directly above and to a shallow northeast extension corresponding to the Matsukawa geothermal area. The low resistivity area is most likely indicative of magmatic fluids, such as supercritical water or melts, as previously described. If the conductive body indicates a high-temperature fluid supply path from the deep subsurface, then the Kakkonda and Matsukawa geothermal areas, which apart approximately 7 km horizontally, may share a common heat source. Kimbara (1983) pointed out that the geothermal areas of Kakkonda and Matsukawa are related, considering the distribution of alteration zones. Indeed, Kimbara (1983) suggested that these two areas share a common heat source with heat supplied directly beneath the Kakkonda geothermal area. Our results support this and further suggest that the deep supply source is located in the southwest. Takahashi et al. (2004) estimated a conductive body (< 100 Ωm) with a diameter of approximately 15 km at 12–22 km below sea level beneath the Akita Komagatake volcano, slightly south of the Eboshidake volcano, based on an 80-km east-west MT survey across this area. Our estimated conductive body is broadly consistent with that proposed by Takahashi et al. (2004); their conductor extends slightly further east at a deeper depth, reaching the Moho discontinuity. Collectively, the conductive bodies, which connect the Moho to the Kakkonda granite, may represent a heat and water supply system containing melts and supercritical geothermal fluids. This is similar to the structures shown at the Naruko volcano (Ogawa et al., 2014) and Shikotsu caldera (Yamaya et al., 2017), which are also located in the Northeast Japan Arc, implying a universal supply system for supercritical geothermal systems in subduction zones.

There are, however, few MT stations near Eboshidake volcano and Mt. Mitsuishi owing to the steep terrain and dense vegetation. Therefore, it is necessary to increase the number of MT stations in these areas to further improve estimations. In addition, Ishizu et al. (2021) used numerical calculations to show that if such conductive columns are found in the inversion analysis, larger conductors may exist at depth. Specifically, these authors' calculations were based on the conductor in the Kakkonda area estimated by Yamaya et al. (2017b), which adopted a similar MT station layout to our study. Therefore, based on similar interpretations, the conductor may extend in the north-south direction at depth, and the geothermal supply system at these depths needs to be carefully examined coupled with additional geophysical data including seismic velocity and/or attenuation distribution assessments.

5. Conclusions

A wideband MT survey was conducted in the eastern part of the Sengan region of

Japan. The resistivity structure estimated by 3-D inversion detected the conductor at an elevation of -1.8 km or deeper in the Kakkonda granite. The hypocenter distribution suggests that the conductor is located in the ductile zone with a temperature above 370 °C. The conductor is also located below the minimum quartz solubility profile of the WD-1a well (Saishu et al., 2014) and may be capped by silica at 380–400 °C or above. This conductor corresponds to two-phase dominant or single-phase type conditions in which supercritical geothermal reservoirs exist, as examined by Watanabe et al. (2021b). The permeability of the supercritical reservoirs was estimated from the resistivity of the conductor by applying the RGPZ equation proposed by Glover et al. (2006). The calculated permeability of the reservoir top surface was estimated to be between 5.0E-17 and 5.0E-15 m^2 or higher, implying that an exploitable supercritical geothermal reservoir exists in the Kakkonda granitic body.

The low-resistivity body may represent magmatic fluids with melts at greater depths. At elevations below -4 km, the conductor extends beneath the active volcano on the southwest side. This is probably a conductive zone connected from the Moho discontinuity and may represent a typical supply system of supercritical geothermal fluids of the Northeast Japan Arc. We also suggest that this supply system could be a heat source not only for the Kakkonda area but also for the Matsukawa area. However, additional MT observation data and evidence from other geophysical sources including seismic velocity structure data are needed to validate our interpretations of these deep structures.

Competing interests

The authors declare no competing interests.

Acknowledgements

We thank Prof. Koki Aizawa from Kyushu University, Dr. Masaaki Mishina formerly from Tohoku University, and Mr. Kosuke Takahashi from the Japan Meteorological Agency for providing the MT data for the Iwate volcano. Prof. Takeshi Hashimoto from Hokkaido University, Prof. Shinya Sakanaka from Akita University, and Dr. Shinichi Takakura from National Institute of Advanced Industrial Science and Technology provided us the MT equipment used in the 2019 survey. Ms. Junna Kanehiro and Mr. Wataru Yamada from Hokkaido University, Mr. Keishi Nunohara from Tohoku University, and Mr. Masato Fukai from the Tokyo Institute of Technology helped us with MT measurements in 2019. The Tohoku Sustainable and Renewable Energy Co. Inc. supported us in carrying out the MT survey and allowed us to use their unpublished well log data. The Geothermal Engineering Co., Ltd. supported the collection and organization of the well log data. Several figures were created using generic mapping tools (GMT) (Wessel et al., 2013).

Funding

This study was part of the supercritical geothermal project funded by the New Energy and Industrial Technology Development Organization (NEDO).

Author contributions

Conceptualization: YY, HA, TM, YO

Planning and preparing the MT survey: YY, YS, YM, HA, HH, TM, YO, and TU

Carrying out the MT survey: YY, YS, YM, KO, HH, YO, and TU

Data analysis: YY, HH, KI, YO, TU

Estimation of permeability: YY, NW, TM, YO, KI

Writing original draft: YY

Discussion, reviewing, and editing of the manuscript: All authors.

References

Aizawa, K., Ogawa, Y., Mishina, M., Takahashi, K., Nagaoka, S., Takagi, N., Sakanaka, S., Miura, T., 2009. Structural controls on the 1998 volcanic unrest at Iwate volcano: Relationship between a shallow, electrically resistive body and the possible ascent route of magmatic fluid. Journal of Volcanology and Geothermal Research, 187, 131–139. https://doi.org/10.1016/j.jvolgeores.2009.08.009.

Archie, G.E., 1942. The electrical resistivity log as an aid in determining some reservoir characteristics. Transactions of the American Institute of Mechanical Engineers, 146, 54–67.

Bertrand, E.A., Caldwell, T.G., Bannister, S., Soengkono, S., Bennie, S.L., Hill, G.J., Heise, W., 2015. Using array MT data to image the crustal resistivity structure of the southeastern Taupo Volcanic Zone, New Zealand. Journal of Volcanology and Geothermal Research, 305, 63–75. https://doi.org/10.1016/j.jvolgeores.2015.09.020.

Chave, A.D., and D.J., Thomson, 2004. Bounded influence estimation of magnetotelluric response functions. Geophysical Journal International, 157, 988–1006.

Doi, N., Kato, O., Ikeuchi, K., Komatsu, R., Miyazaki, S., Akaku, K., Uchida, T., 1998. Genesis of the plutonic-hydrothermal system around quaternary granite in the kakkonda geothermal system, Japan. Geothermics, 27, 663– 690.

Doi, N., Kasai, K., Sakagawa, Y., Shigehara, S., Kato, O., Takahashi, M., Koide, K., Tosha, T., 2001. Geothermal reservoir of the Kakkonda, Iwate prefecture, Japan. Volcanic Structure in the Shallow Part and Volcanic Fluid, Conference report of Disaster Prevention Research Institute Kyoto University, 12K-3, 89–100.

Friðleifsson, G.Ó., Elders, W.A., Zierenberg, R.A., Stefánsson, A., Fowler, A.P.G., Weisenberger, T.B., Harðarson, B.S., Mesfin, K.G., 2017. The Iceland Deep Drilling Project 4.5 km deep well, IDDP-2, in the seawater-recharged Reykjanes geothermal field in SW Iceland has successfully reached its supercritical target. Scientific Drilling, 23, 1–12. https://doi.org/10.5194/sd-23-1-2017.

Fournier, R.O., 1999. Hydrothermal processes related to movement of fluid from plastic into brittle rock in the magmatic-epithermal environment. Economic Geology, 94(8), 1193. http://dx.doi.org/10.2113/gsecongeo.94.8.1193.

Fujimoto, K., Takahashi, M., Doi, N. and Kato, O., 2000. High permeability of Quaternary granites in the Kakkonda geothermal area, northeast Japan. World Geothermal Congress 2000, Kyushu, Japan.

Gamble, T.D., Goubau, W.M., Clarke, J., 1979. Error analysis for remote reference magnetotellurics. Geophysics, 44, 864–992. https://doi.org/10.1190/1.1440988.

Glover, P.W.J., Zadjali, I.I., Frew, K.A., 2006. Permeability prediction from MICP and NMR data using an electrokinetic approach. Geophysics, 71(4), F49–F60.

Hanano, M., 1995. Review of recent development of the Kakkonda deep reservoir, Japan. Proc. World Geothermal Congress, 95, 1629–1634.

Hanano, M. and Matsuo, G., 1990. Initial State of the Matsukawa Geothermal Reservoir: Reconstruction of a Reservoir Pressure Profile and its Implications. Geothermics, 19, 541–560.

Hata, M., Matsushima, N., Takakura, S., Utsugi, M., Hashimoto, T., Uyeshima, M., 2018. Three-dimensional electrical resistivity modeling to elucidate the crustal magma supply system beneath Aso caldera, Japan. Journal of Geophysical Research: Solid Earth, 123, 6334– 6346. https://doi.org/10.1029/2018JB015951.

Ichihara, H., Sakanaka, S., Mishina, M., Uyeshima, M., Nishitani, T., Ogawa, Y., Yamaya, Y., Mogi, T., Amita, K., Miura, T., 2014. A 3-D electrical resistivity model beneath the focal zone of the 2008 Iwate-Miyagi Nairiku earthquake (M 7.2). Earth, Planets and Space, 66, 50. https://doi.org/10.1186/1880-5981-66-50.

Ishizu, K., Ogawa, Y., Mogi, T., Yamaya Y., Uchida, T., 2021. Ability of the magnetotelluric method to image a deep conductor: Exploration of a supercritical geothermal system. Geothermics, 96, 102205. https://doi.org/10.1016/j.geothermics.2021.102205.

Ishizu, K., Ogawa, Y., Nunohara, K., Tsuchiya, N., Ichiki, M., Hase, H., Kanda, W., Skanaka, S., Honkura, Y., Hino, Y., Seki, K., Tseng, K.H., Yamaya, Y., Mogi, T., 2021. Estimation of spatial distribution and fluid fraction of a potential supercritical geothermal reservoir by magnetotelluric data: a case study from Yuzawa geothermal field, NE Japan. Earth and Space Science Open Archive. https://doi.org/10.1002/essoar.10507736.1.

Kanisawa, S., Doi, N., Kato, I., Ishikawa, K., 1994. Quaternary Kakkonda Granite underlying the Kakkonda Geothermal Field, Northeast Japan. Journal of Mineralogy, Petrology and Economic Geology, 89, 390–407. https://doi.org/10.2465/ganko.89.390.

Karlsdóttir, R., Vilhjálmsson, A.M., Guðnason, E.Á., 2020. Three dimensional inversion of magnetotelluric (MT) resistivity data from Reykjanes high temperature field in SW Iceland. Journal of Volcanology and Geothermal Research, 391, 106498, https://doi.org/10.1016/j.jvolgeores.2018.11.019.

Kato, O., Doi, N., Sakagawa, Y., Uchida, T., 1998. Fracture systematics in and around well WD-1, Kakkonda geothermal field, Japan. Geothermics, 27, 609–629.

Kelbert A., Meqbel N., Egbert G.D., Tandonc K., 2014. ModEM: a modular system for inversion of electromagnetic geophysical data. Computational Geosciences, 66, 40–53. https://doi.org/10.1016/j.cageo 2014, 01: 010.

Kimbara, K., 1983. Hydrothermal rock alteration and geothermal systems in the eastern Hachimantai geothermal area, Iwate Prefecture, northern Japan. Journal of the Japanese Association of Mineralogists, Petrologists and Economic Geologists, 78, 479–490. https://doi.org/10.2465/ganko1941.78.479.

Lee B., Unsworth, M., Árnason, K., Cordell, D., 2020. Imaging the magmatic system beneath the Krafla geothermal field, Iceland: A new 3-D electrical resistivity model from inversion of magnetotelluric data. Geophysical Journal International, 220, 541–567. https://doi.org/10.1093/gji/ggz427.

New Energy Development Organization, 1983. Development Promotion Survey Report, No. 1, Hachimantai-toubu area, 614pp.

New Energy and Industrial Technology Development Organization, 1990. Report of Nationwide Geothermal Resources Exploration Project (3rd Phase) in FY 1990, Regional Exploration of Geothermal Fluid Circulation System, Akitakoma area, Resistivity (MT and AMT method), 253pp.

New Energy and Industrial Technology Development Organization, 1991. Development of Hydrothermal Power Plants (Development of Technology for increasing geothermal energy recovery), FY1990 Report on the Results of the Sunshine Project, 659pp.

New Energy and Industrial Technology Development Organization, 1992a. Development of Hydrothermal Power Plants (Development of Technology for increasing geothermal energy recovery), FY1991 Report on the Results of the Sunshine Project, 659pp.

New Energy and Industrial Technology Development Organization, 1992b. Geothermal Development Promotion Survey Report, No. 27, Tazawako-toubu area, 1021pp.

New Energy and Industrial Technology Development Organization, 1993. Geothermal Development Promotion Survey Report. No. 31, Iwatesan-seibu area, 1289pp.

New Energy and Industrial Technology Development Organization, 1998. Report on Verification of Geothermal Exploration Technologies in FY 1996, Deep-seated geothermal resources survey, 948pp.

New Energy and Industrial Technology Development Organization, 1999. Report on Verification of Geothermal Exploration Technologies in FY 1998, Deep-seated geothermal resources survey, 1118pp.

NOAA National Geophysical Data Center, 2009. ETOPO1 1 Arc-Minute Global Relief Model. NOAA National Centers for Environmental Information. Accessed Aug. 15, 2021. http://dx.doi.org/10.7289/V5C8276M.

Ogawa, Y., Uchida, T., Takakura, S., 1997. Survey on the resistivity structure of the Kakkonda geothermal field, NE Japan (1). Proceedings of the 1997 Conductivity Anomaly Symposium, 182–188.

Ogawa, Y., Ichiki, M., Kanda, W., Mishina M., Asamori, K., 2014. Three-dimensional magnetotelluric imaging of crustal fluids and seismicity around Naruko volcano, NE Japan. Earth, Planets and Space, 66, 158. https://doi.org/10.1186/s40623-014-0158-y.

Okamoto, K., Asanuma, H., Ishibashi, T., Yamaya, Y., Siashu, H., Yanagagisawa, N., Mogi, T., Tsuchiya, N., Okamoto, A., Naganawa, S., Ogawa, Y., Ishitsuka, K., Fujimitsu, Y., Kitamura, K., Kajiwara, T., Horimoto, S., Shimada K., 2019, Geological and engineering features of developing ultra-high-temperature geothermal systems in the world. Geothermics 82, 267–281.

Okamoto, K., Imanishi, K., Asanuma, H., 2021. Structures and fluid flows inferred from microseismic events around a low-resistivity anomaly in Kakkonda Geothermal Field, NE Japan. Geothermics (under review for this special issue).

Reinsch, T., Dobson, P., Asanuma, H., Huenges, E., Poletto, F., Sanjuan, B., 2017. Utilizing supercritical geothermal systems: a review of past ventures and ongoing research activities. Geothermal Energy, 5, 16.

Rung-Arunwan, T., Siripunvaraporn, W., Utada, H., 2017. Use of ssq rotational invariant of magnetotelluric impedances for estimating informative properties for galvanic distortion. Earth, Planets and Space, 69, 80. https://doi.org/10.1186/s40623-017-0665-8.

Siripunvaraporn, W., Egbert, G., 2000. An efficient data-subspace inversion method for 2-D magnetotelluric data. Geophysics, 65, 791–803. https://doi.org/10.1190/1.1444778.

Siripunvaraporn, W., Egbert, G., Lenbury, Y., Uyeshima, M., 2005. Three-dimensional magnetotelluric inversion: Data-space method. Physics of the Earth and Planetary Interiors, 150, 3–14.

Siripunvaraporn, W., Egbert, G., 2009. WSINV3DMT: Vertical magnetic field transfer function inversion and parallel implementation. Physics of the Earth and Planetary Interiors, 173, 317–329.

Uchida, T., Ogawa, Y., Takakura, S., Mitsuhata, Y., 2000. Geoelectrical investigation of the Kakkonda geothermal field, northern Japan. Proceedings World Geothermal Congress 2000, 1893–1898.

Uchida, T., Lee, T. J., Cerv, V., 2003. 3-D inversion of magnetotelluric data in the Kakkonda geothermal field, northern Japan. Proceedings of 6th SEGJ International Symposium, 274–280.

Usui, Y., 2015. 3-D inversion of magnetotelluric data using unstructured tetrahedral elements: applicability to data affected by topography. Geophysical Journal International, 202(2): 828–849. https://doi.org/10.1093/gji/ggv186.

Usui, Y., Ogawa, Y., Aizawa, K., Kanda, W., Hashimoto, T., Koyama, T., Yamaya, Y., Kagiyama, T., 2017. Three-dimensional resistivity structure of Asama Volcano revealed by data-space magnetotelluric inversion using unstructured tetrahedral elements. Geophysical Journal International, 208(3), 1359–1372. https://doi.org/10.1093/gji/ggw459.

Takahashi, K., Mishina, M., Hamagushi, H., Mogi, T., 2004. Resistivity structure of the deep-low-frequency earthquake zone near Iwate Volcano. Proceedings of the 2003 Conductivity Anomaly Symposium, 40–47.

Tseng, K-H, Ogawa, Y., Nurhasan, Tank, S.B., Ujihara, N., Honkura, Y., Terada, A., Usui, Y., Kanda, W., 2020. Anatomy of Active Volcanic Edifice at the Kusatsu-Shirane Volcano, Japan, by Magnetotellurics: Hydrothermal Implications for Volcanic Unrests. Earth, Planets and Space, 72, 161. https://doi.org/10.1186/s40623-020-01283-2.

Watanabe, N., Yamaya, Y., Kitamura, K., Mogi, T., 2021a. Viscosity-dependent empirical formula for electrical conductivity of H_2O-NaCl fluids at elevated temperatures and high salinity. Fluid Phase Equilibria, 549, 113187. https://doi.org/10.1016/j.fluid.2021.113187.

Watanabe, N., Mogi, T., Yamaya, Y., Kitamura, K., Asanuma, H., Tsuchiya, N., 2021b. Electrical conductivity of fluids in superhot geothermal reservoirs within granitic intrusions: Constraints from the phase relations of a H2O-NaCl system. Geothermics (under review for this special issue)

Wessel P., Smith, W.H, Scharroo, R., Luis, J., Wobbe, F., 2013. Generic mapping tools: improved version released. EOS Transactions of the American Geophysical Union, 94(45), 409–410. https://doi.org/10.1002/2013EO450001.

Yamaya, Y., Mogi, T., Honda, R., Hase, H., Hashimoto, T., Uyeshima, M., 2017a. Three-dimensional resistivity structure in Ishikari Lowland, Hokkaido, northeastern Japan—Implications to strain concentration mechanism. Geochemistry, Geophysics, Geosystems, 18, 735–754. https://doi.org/10.1002/2016GC006771.

Yamaya, Y., Uchida, T., Ogawa, Y., Mogi, T., 2017b. Organization of resistivity exploration data for development of deep geothermal systems—Reprocessing magnetotelluric data from the Kakkonda geothermal field, northeast Japan. Proceedings of 39th NZ geothermal workshop, no.061.

Yanagisawa, N., Masuda, Y., Asanuma, H., Osato, K., Sakura, K., 2021. Estimation of casing material corrosion rates for supercritical geothermal development. Geothermics, 96, 102149. https://doi.org/10.1016/j.geothermics.2021.102149.

Tsuchiya, N., Yamada, R., Uno, M., 2016. Supercritical geothermal reservoir revealed by a granite–porphyry system. Geothermics, 63, 182–194. https://doi:10.1016/j.geothermics.2015.12.011.

Figures

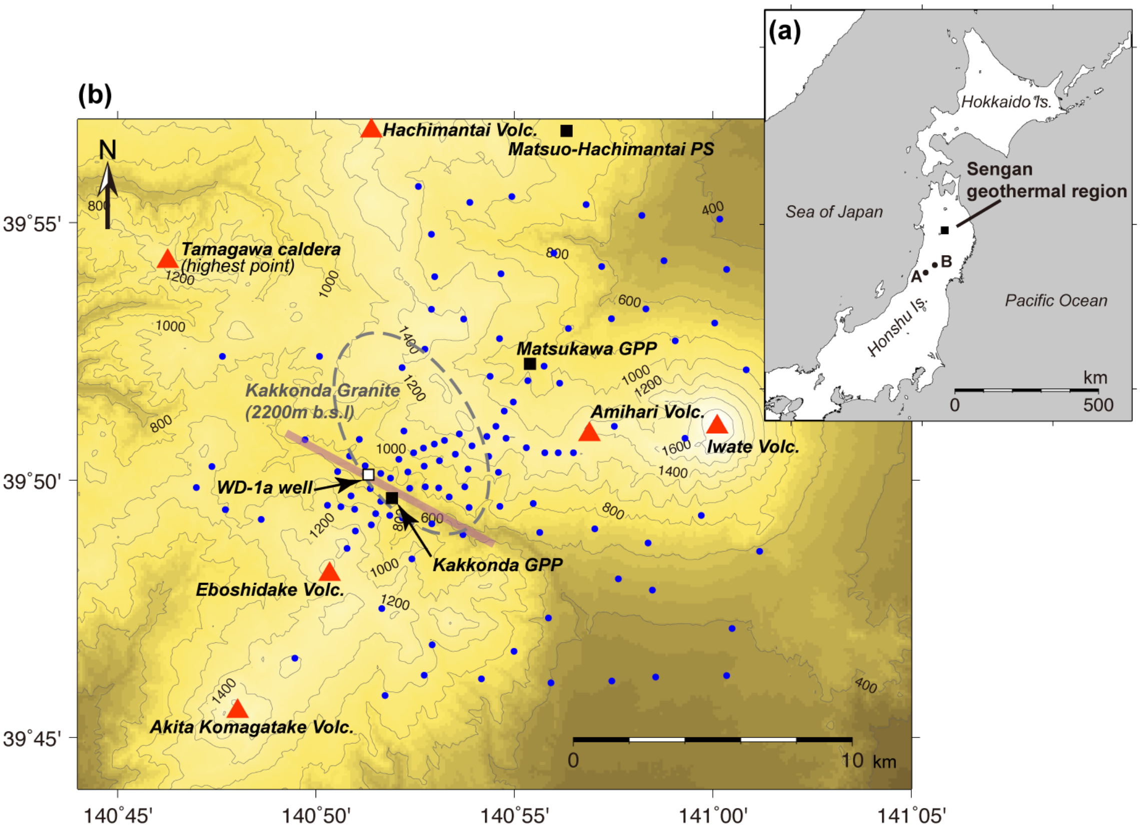

Fig. 1: (a) Location of the Sengan geothermal region. Black dots indicate the remote stations used for the remote reference processing. (b) Location map of the study area. Blue dots indicate MT stations. Red triangles indicate Quaternary volcanoes. Black squares indicate geothermal power stations. The white square indicates the WD-1a well. The gray dashed line represents the outline of the estimated Kakkonda granite at 2,200 m below sea level after Doi (2001). The pink line indicates the resistivity profile shown in Fig. 10. Topography is based on the 10 m mesh DEM provided by the Geospatial Information Authority of Japan.

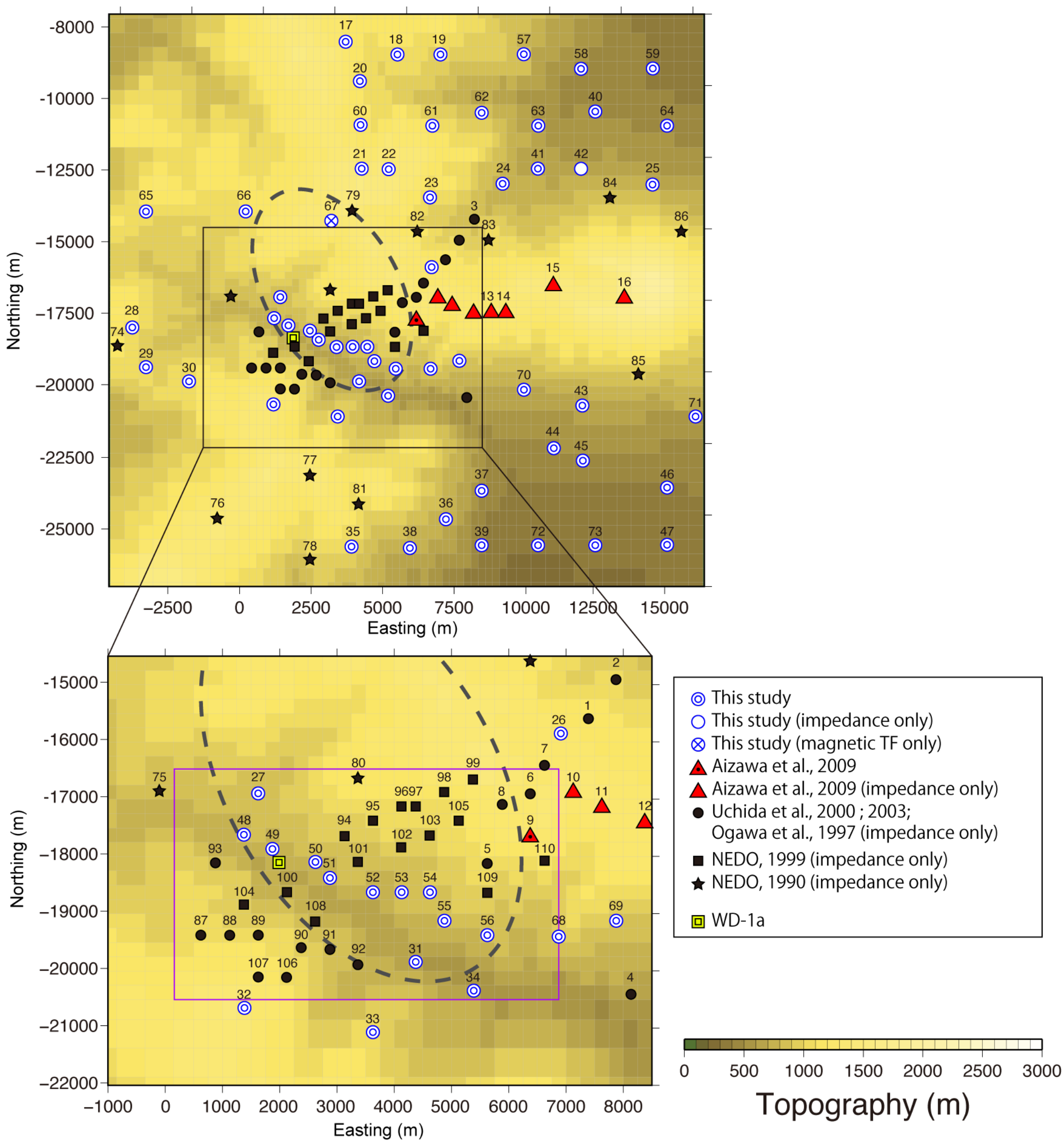

Fig. 2: MT stations and horizontal grid used for 3-D inversion analysis. The purple rectangle in the lower panel indicates the area analyzed by Yamaya et al. (2017). The gray dashed line represents the outline of the estimated Kakkonda granite at 2,200 m below sea level after Doi (2001).

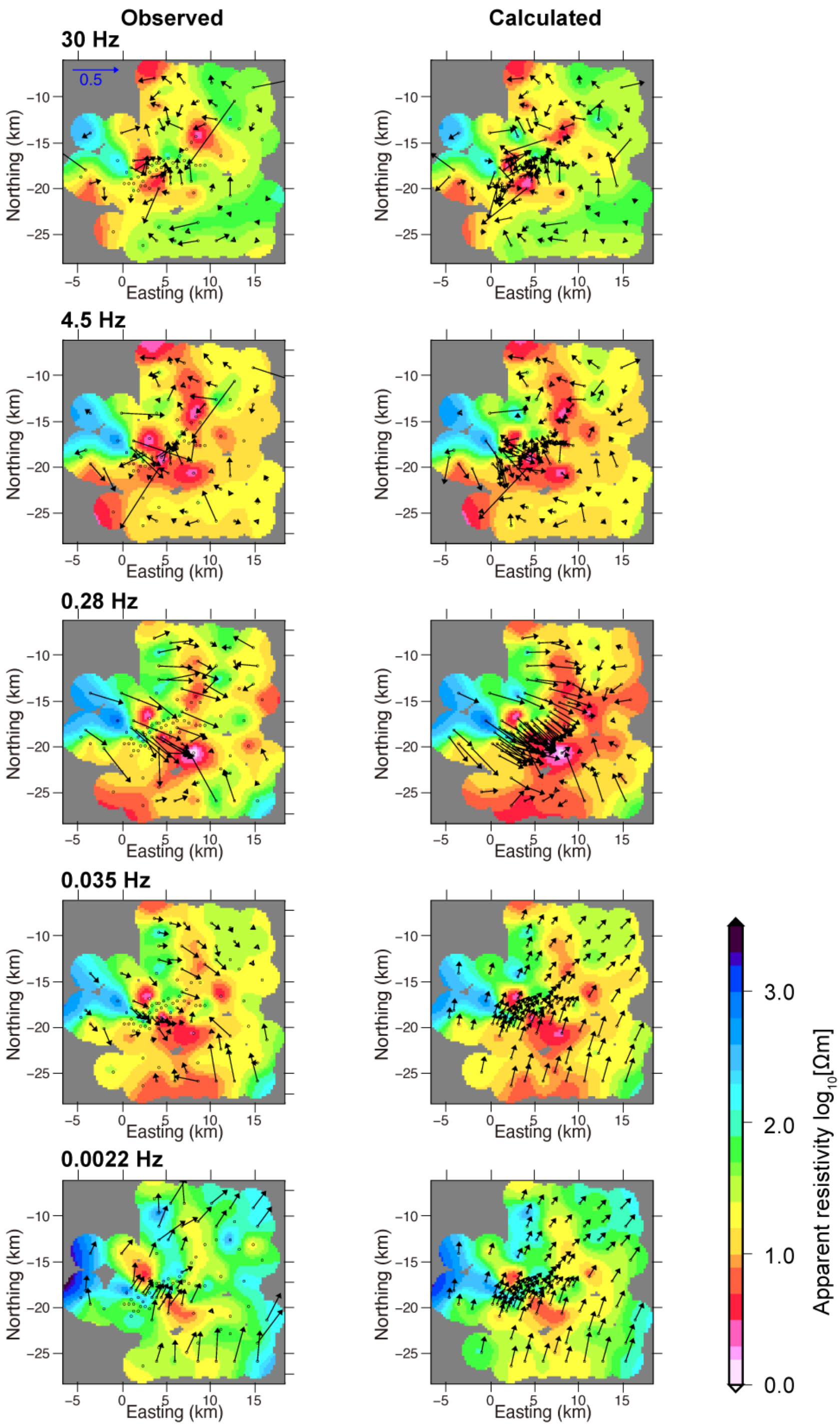

Fig. 3: Apparent resistivity based on the SSQ invariant impedance and the real part of the induction vector (Parkinson's convention) of the observed data (left) and that of the calculated from the final model (right). The observed induction vector is shown only at the station that measured the three components of the magnetic fields. Half a unit induction vector is shown in the "Observed" 30 Hz panel.

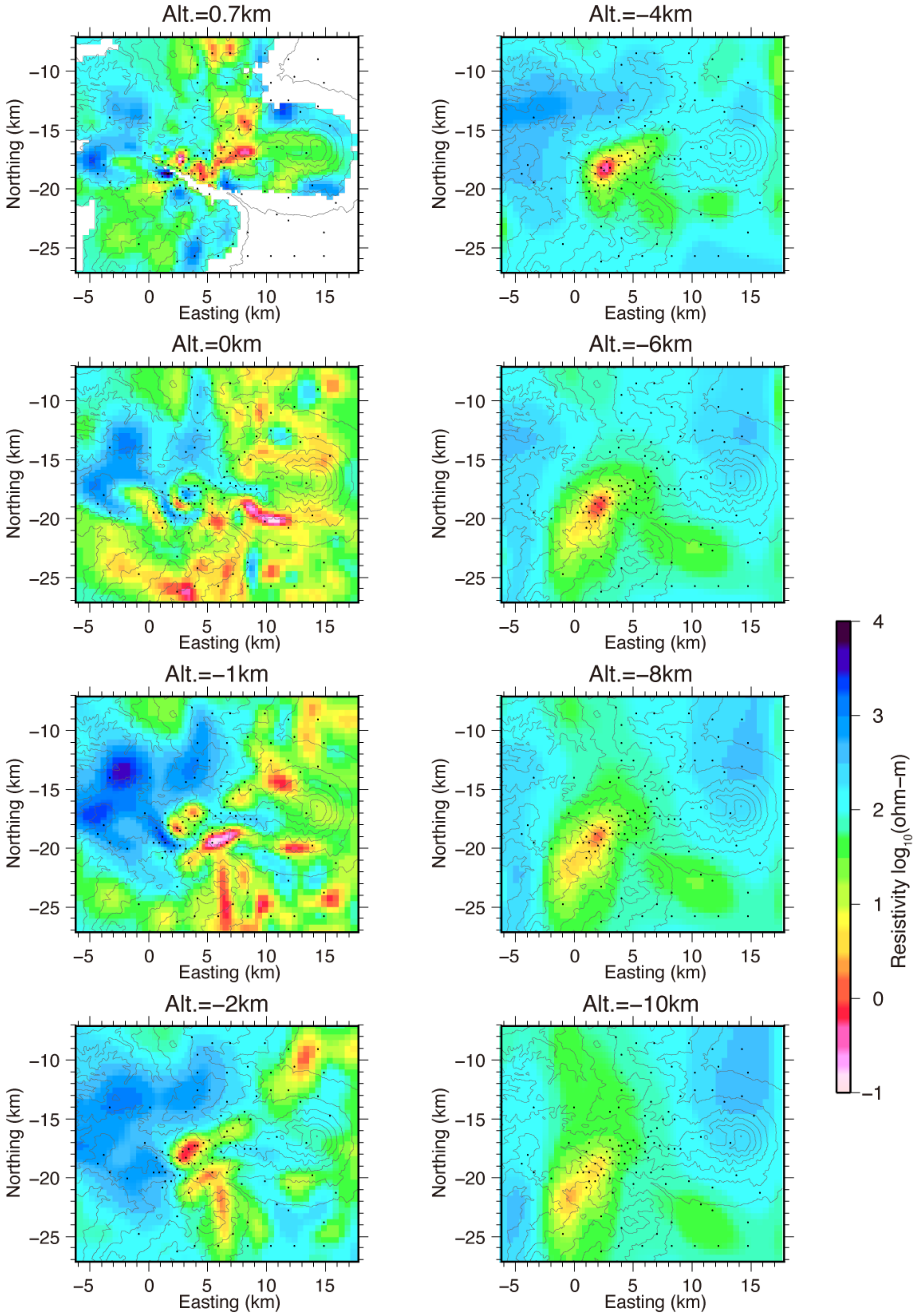

Fig. 4: Plan view of the resistivity model. The black dots indicate the MT stations.

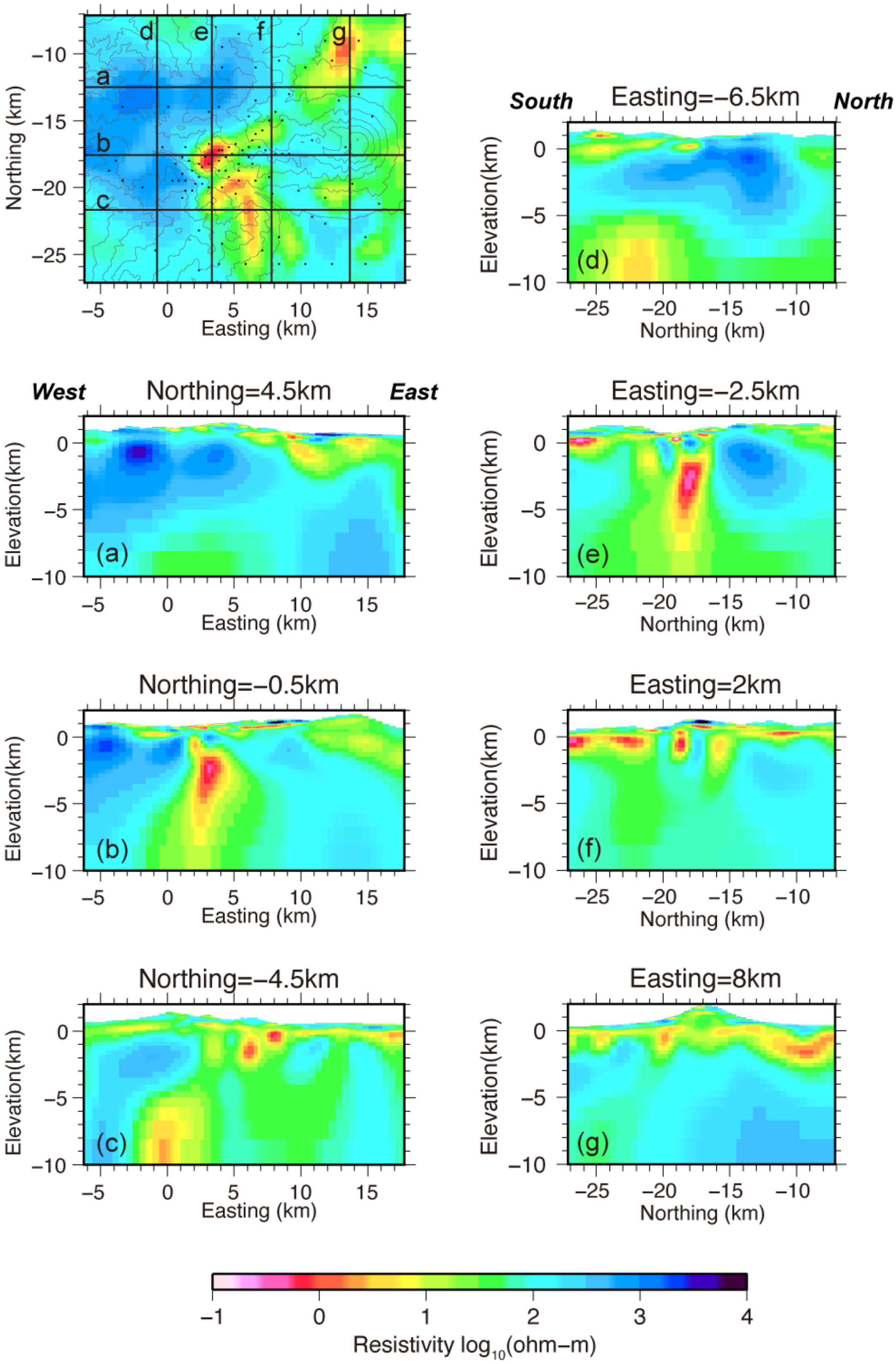

Fig. 5: Resistivity sections along west-east (a–c) and south-north (d–g) profiles.

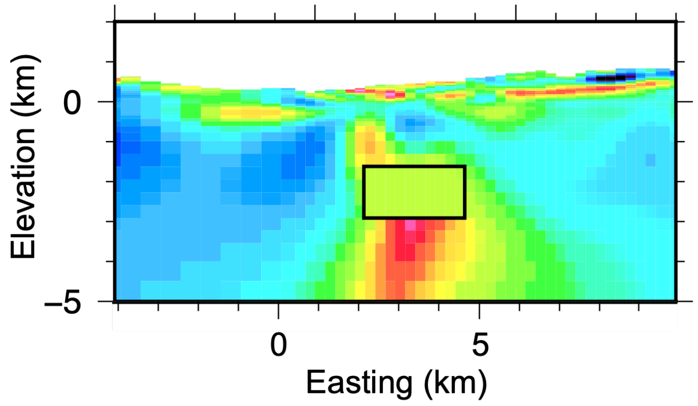

Fig. 6: Area where resistivity was fixed in the sensitivity tests.

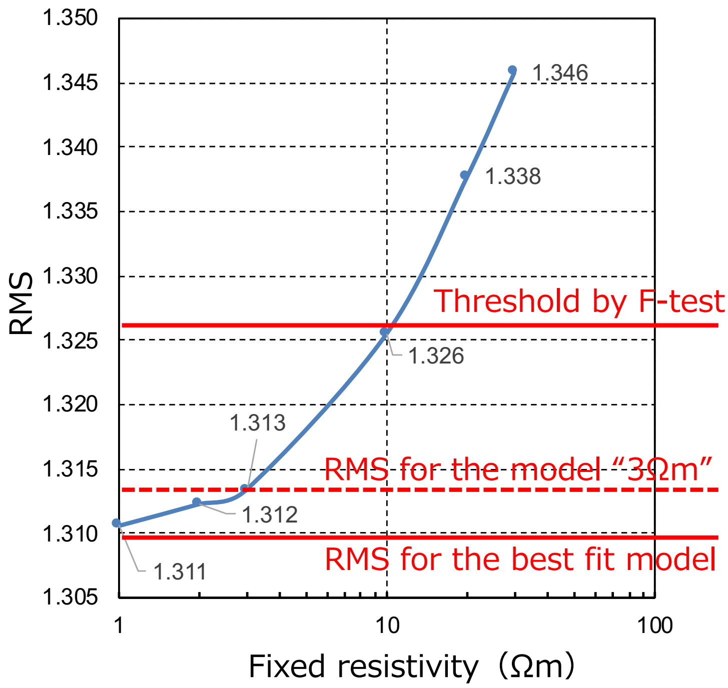

Fig. 7: RMS misfit with respect to the fixed resistivity values in the sensitivity tests.

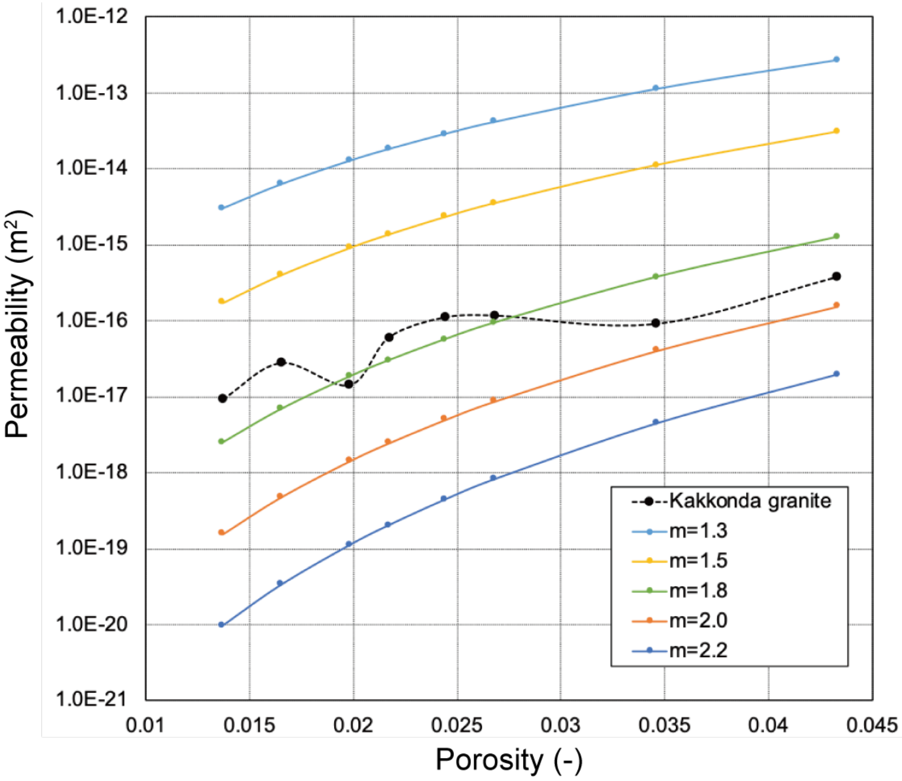

Fig. 8: Relationship between permeability and porosity based on the RGPZ equation. Grain size was assumed as $d = 1$ mm. The black dots indicate data obtained in laboratory measurements (NEDO, 1998; Fujimoto et al., 2000).

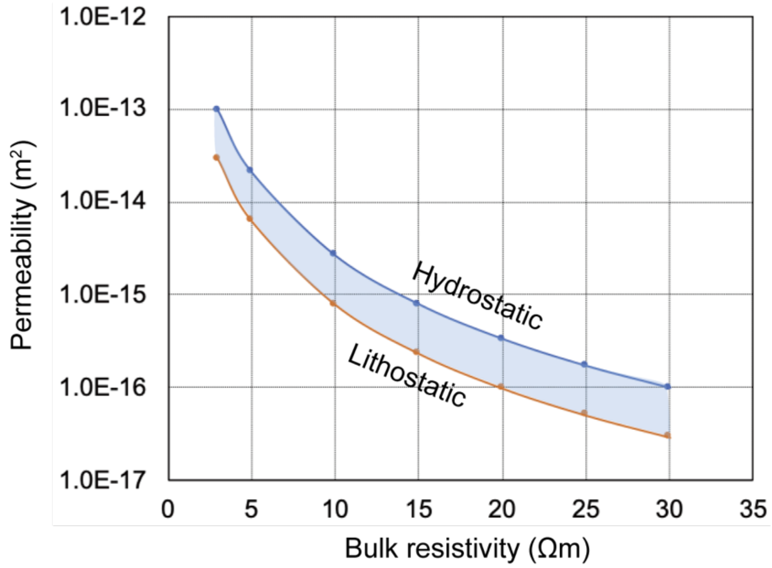

Fig. 9: Predicted permeability of supercritical reservoirs with respect to bulk resistivity.

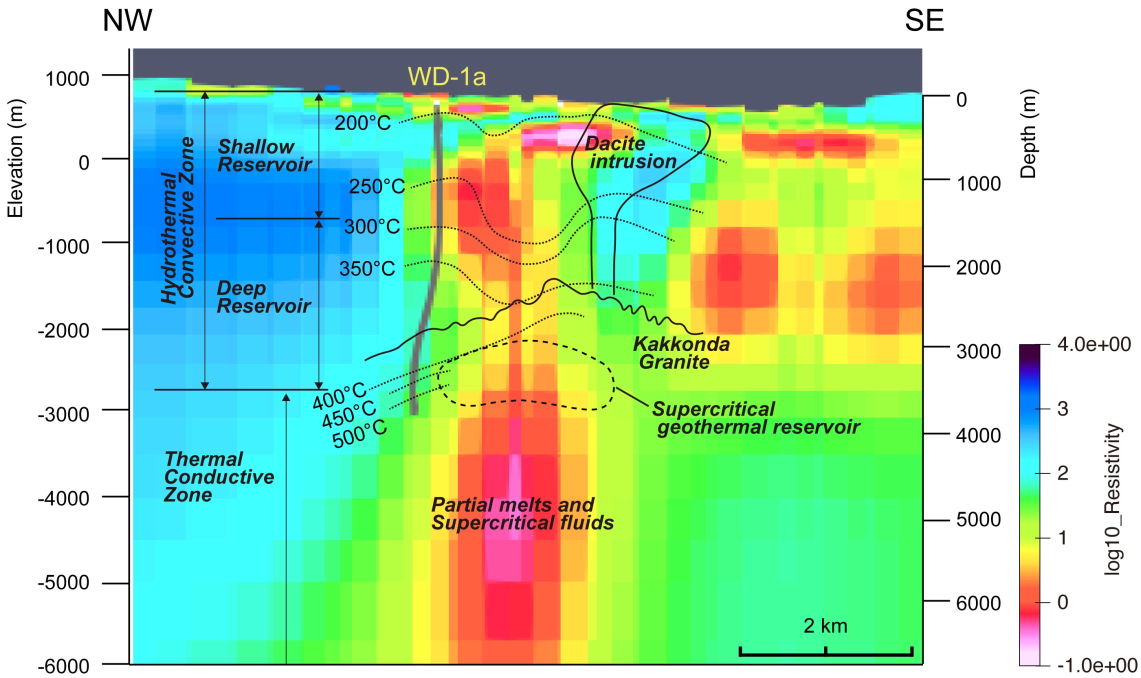

Fig. 10: Resistivity cross-section and its interpretation along a NW-SE profile (shown in Fig. 1) crossing the Kakkonda geothermal field. Geology, temperature, and reservoir types are superimposed after Doi et al. (1998). The solid gray line indicates the trace of the WD-1a well.

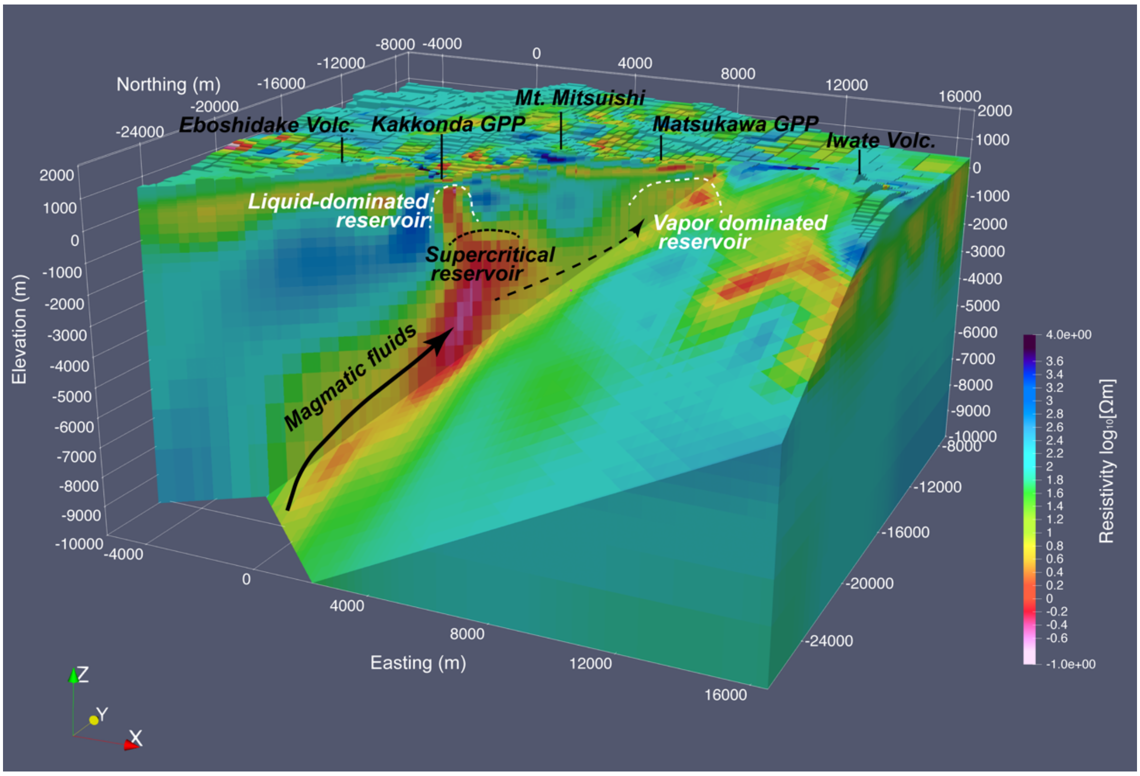

Fig. 11: Cutaway model of the resistivity structure and interpretation of the heat-supplying system in the Sengan geothermal region.